Molecular Gating of Silicon Nanowire Field-Effect Transistors with Nonpolar Analytes

Yair Paska,[†] Thomas Stelzner,[‡] Ossama Assad,[†] Ulrike Tisch,[†] Silke Christiansen,[‡,§] and Hossam Haick[†,*]

[†]The Department of Chemical Engineering and Russell Berrie Nanotechnology Institute, Technion—Israel Institute of Technology, Haifa 32000, Israel, [‡]Institute of Photonic Technology e.V., Albert-Einstein-Straße 9, 07745 Jena, Germany, and [§]Max-Planck-Institute for the Science of Light, Günther-Scharowsky-Straße 1, 91058 Erlangen, Germany

ABSTRACT Silicon nanowire field-effect transistors (Si NW FETs) have been used as powerful sensors for chemical and biological species. The detection of polar species has been attributed to variations in the electric field at the conduction channel due to molecular gating with polar molecules. However, the detection of nonpolar analytes with Si NW FETs has not been well understood to date. In this paper, we experimentally study the detection of nonpolar species and model the detection process based on changes in the carrier mobility, voltage threshold, off-current, off-voltage, and subthreshold swing of the Si NW FET. We attribute the detection of the nonpolar species to molecular gating, due to two *indirect* effects: (i) a change in the dielectric medium close to the Si NW surface and (ii) a change in the charged surface states at the functionality of the Si NW surface. The contribution of these two effects to the overall measured sensing signal is determined and discussed. The results provide a launching pad for real-world sensing applications, such as environmental monitoring, homeland security, food quality control, and medicine.

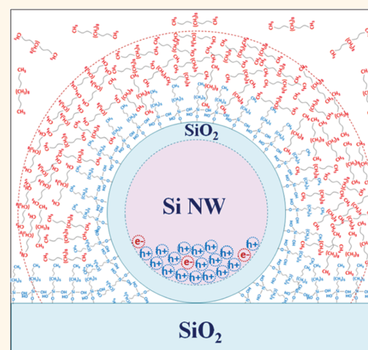

KEYWORDS: silicon · nanowire · transistor · sensor · molecular gating

Silicon nanowires (Si NWs) have been successfully employed for both gas[1−3] and liquid[4−8] phase sensing. Si NWs are generally used as field-effect transistors (FETs), though chemiresistors based on Si NWs have also been demonstrated.[9,10] Chemiresistors are relatively cheap to fabricate and operate. However, reusability is rather limited, mainly because they cannot be regenerated easily. Using Si NW FETs provides a distinct advantage over competing strategies. This could be attributed to (i) the relatively straightforward conductance measurements; (ii) the ability to optimize the sensing response by applying an optimum gate voltage(s);[2,11] and (iii) the ability to control the electrical properties and effective analyte delivery to the Si NWs by means of molecular engineering with organic molecules.[4,12−15] Added key advantages are the low power consumption (on the order of tens of nW per nanowire) and the prospect of extreme miniaturization.[8]

Impressive progress has been made in sensing polar analytes with Si NW FET sensors, using variations of electrical conductivity measurements[2−8] and organic functionalization that have strong electronic interaction with the target polar analytes. Oxide-coated Si NW FETs were functionalized with amino siloxanes to impart relatively high sensitivity toward pH, and with a variety of biological receptors to impart selectivity toward biological species in solution.[3,4,6−8] Similar approaches were used for achieving highly sensitive detection of polar analytes in the gas phase (*e.g.*, N_2O, NO, CO).[3] It is widely accepted that the conductance of (molecularly modified) Si NW FET sensors changes in response to variations in the electric field or the potential at the conduction channel's outer surface that result from molecular gating, viz., the binding or adsorption of (bio)-molecules.[1,16,17] The analyte molecules' polarity is believed to dominate their interaction with the surface of the Si NW and, in turn, the conduction inside the Si NW FET.[1,2,18−21] Various electrostatic effects can cause this molecular gating,[22] for example, adsorption of charged molecules[23] or effective charging of the surface due to the adsorption process.[24] In addition, adsorption of a molecular monolayer can create a surface dipole, which changes the surface electron affinity and, consequently, its work function, depending on the dipole orientation and magnitude.[14]

In contrast to the detection of polar analytes, the detection of nonpolar analytes with molecularly modified Si NW FETs still remains

* Address corresponding to hhossam@technion.ac.il.

Received for review September 23, 2011 and accepted December 16, 2011.

Published online December 16, 2011
10.1021/nn203653h

© 2011 American Chemical Society

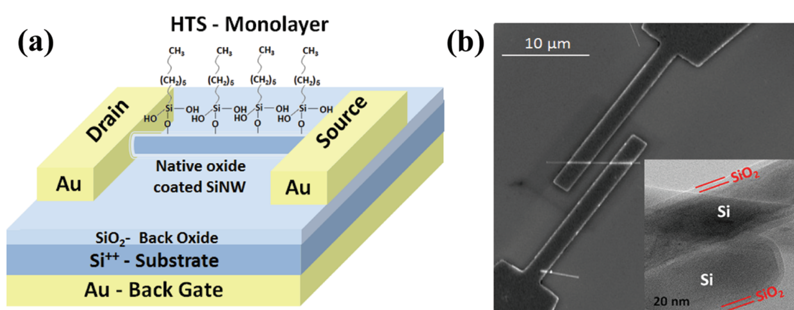

Figure 1. (a) Schematic representation of the HTS-Si NW FET. (b) Scanning electron microscope (SEM) image of a representative Si NW FET test device that was modified with HTS functionality. Inset: Transmission electron microscopy (TEM) image of a representative Si NW.

challenging and limits their widespread use in real-world applications such as environmental monitoring, homeland security, quality control in the food industry, or medical sensing.[1] Recently, we have used a tailor-made organic functionalization and recorded electrical response of Si NW FETs with high signal-to-noise ratio upon exposure to nonpolar analytes.[2] Moreover, we have assigned the observed conductance changes to the exposure to nonpolar analytes, even in real confounding environments with high, fluctuating levels of humidity as well as "fouling" nonspecific binding.[2] The observed molecular effects were explained by *indirect* analyte–functionality interactions, whereby steric changes in the functional groups (or receptors) attached to the Si NW surface affected (i) the dielectric constant and/or effective dipole moment of the organic monolayer and/or (ii) the density of charged surface states at the SiO_2/monolayer interface. Nevertheless, suitable experimental evidence and modeling relating the Si NW FET characteristics with *in situ* physical and electrical measurements have been lacking.

In this study, we combine quartz crystal microbalance (QCM), spectroscopic ellipsometry (SE), Kelvin probe (KP), and electrical measurements with device modeling to explore the interaction of the nonpolar analytes with the Si NW FET. Additionally, we explored whether the sensing was due to a single effect or a combination of effects. The results provided clear evidence for the leading role of molecular gating in detecting nonpolar analytes with Si NW FETs. The origin of molecular gating and the underlying physical principles are discussed in light of the fundamental parameters of the FET characteristics (carrier mobility, voltage threshold, subthreshold swing, off-current, off-voltage, and others).

RESULTS

Individual hexyltrichlorosilane (HTS)-modified Si NW FETs (Figure 1) were tested when exposed to reference air and to noninteracting, nonpolar analytes under 15% RH; see Methods. The background humidity was introduced as a real-world confounding factor.[25] Three nonpolar analytes were examined in the current study (see Table 1). However, for the sake of clear presentation, we focus on decane, as it had the highest response, sensitivity, and detection limit, compared to octane and hexane.[2]

TABLE 1. Physical Properties of the Analytes Used for the Exposure Experiments[26]

analyte	formula	p_o[a] (Torr)	k[b]	n_∞[c]	dipole (D)	density (g·cm^{-3})	volume (Å^3)
n-hexane	$CH_3(CH_2)_4CH_3$	150	1.88	1.37	0	0.655	113.0
n-octane	$CH_3(CH_2)_6CH_3$	14	1.94	1.39	0	0.703	146.6
n-decane	$CH_3(CH_2)_8CH_3$	1.4	1.98	1.41	0	0.730	180.2

[a] p_o stands for the analyte's vapor pressure at 25 °C. [b] k stands for the dielectric constant of the analyte at 20 °C. [c] n_∞ stands for the electronic part of the refractive index of the analyte at 20 °C.

Sensing Characteristics of HTS-Si NW FETs. Figure 2 shows the source–drain current (I_{ds}) *versus* back-gate voltage (V_{bgs}) characteristics of a typical test device during an exposure cycle. As seen in Figure 2a, the I_{ds} values obtained upon exposure to reference air and decane, disregarding the decane's concentration, were similar at V_{bgs} = −30 to −40 V. The I_{ds} decreased at positive V_{bgs} and upon increasing the decane concentration (see also Supporting Information, Figure 1S).[1] The gate voltage that characterized the I_{off} (V_{off}) was slightly shifted to negative V_{bgs} (up to ~3 V shift in V_{off}) under different concentrations of decane, even though the off-current (I_{off}) *per se* preserved its original magnitude (~7×10^{-12}A); see Figure 2b. The subthreshold (10^{-10}–10^{-8}A) slope of the log I_{ds}–V_{bgs} was almost constant (see also Supporting Information, Figure 1S). At 76 ppm decane, the I_{ds}–V_{bgs} characteristics at different exposure periods exhibited similar shapes, but showed significant shifts toward negative V_{bgs} (shifts up to ~13 V after 3 h of exposure). As seen in Figure 2b, the I_{off} decreased systematically (*i.e.*, up to 3×10^{-13}A) and the V_{off} shifted systematically to a more negative V_{bgs}, *i.e.*, shifts up to ~15 V, under similar exposure conditions. The subthreshold (10^{-10} to 10^{-8} A) slope of the log I_{ds}–V_{bgs} in this region increased from 0.136 to 0.195 log(*A*)/V (see Supporting Information, Figure 2S). In a complementary experiment, a bare Si

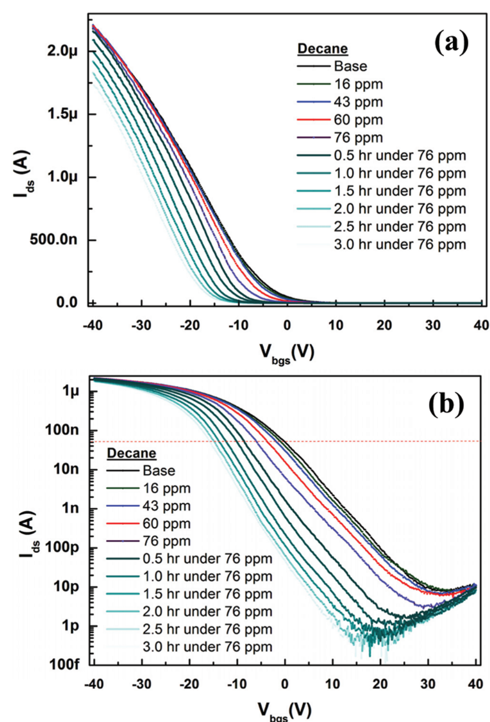

Figure 2. $I_{ds}-V_{bgs}$ measurements under the three sequential exposure steps: (i) reference air; (ii) various decane concentrations; and (iii) constant decane concentration over time, presented in (a) linear scale and (b) log scale.

NW FET that was exposed to reference air exhibited unstable electrical characteristics over time (on a scale of hours). Once stabilized, no response to decane could be obtained (not shown).

In principle, the analysis of the fundamental parameters of the HTS-Si NW FET could be carried out similar to the analysis of planar silicon-on-insulator (SOI) FETs if the different aspects in the device configuration are considered. In the SOI FET configuration,[27] the monolayer is attached to the topmost *planar* SiO_2 layer of the device. This way, the monolayer and/or the analytes affect the channel only from the top, unless a double-gate configuration[28] is used. In the Si NW FET configuration, the monolayer is attached *all around* the oxide sheath of the cylindrical channel, as a gate-all-around configuration (see schematics in Figure 3).[29]

The $I_{ds}-V_{bgs}$ characteristics seen in Figure 2 resemble those obtained with a double-gate FET (*cf.* ref 30). In a double-gate FET structure, one of the gate electrodes is used as the drive gate and the second gate electrode is used as a supplementary gate that pins the channel potential at a fixed voltage.[16,18,19] Therefore, one way to interpret the data in Figure 2 could be to assume that an effective top supplementary gate (*i.e.*, the gate surrounds the periphery of the Si NW) was biased. According to this notion, the effective top gate voltage ($V_{eff\text{-}tg}$) is obtained experimentally from $I_{ds}-V_{bgs}$ characteristics by extracting the back-gate voltage change (ΔV_{bgs}), along a constant I_{ds} level of the reference at V_{bgs} = 0 (50 nA in our case; red line in Figure 2b),

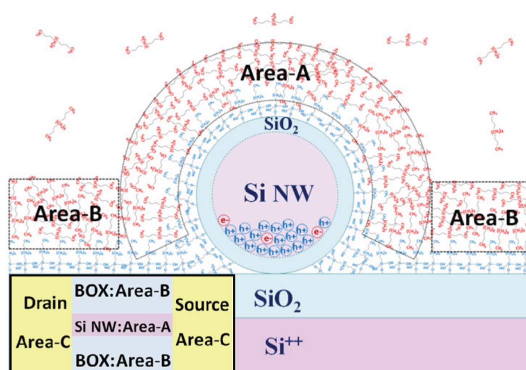

Figure 3. Cross-section schematics of analyte adsorption on the HTS-Si NW FET. Analytes can be adsorbed on three areas of the HTS-Si NW FET device: (i) the Si NW surface (Area-A); (ii) the back-oxide surface of the FET device (Area-B); and (iii) the electrical contacts and/or interface between the Si NW and the electrical contact (Area-C; see inset). Inset: Top view of the HTS-Si NW FET device.

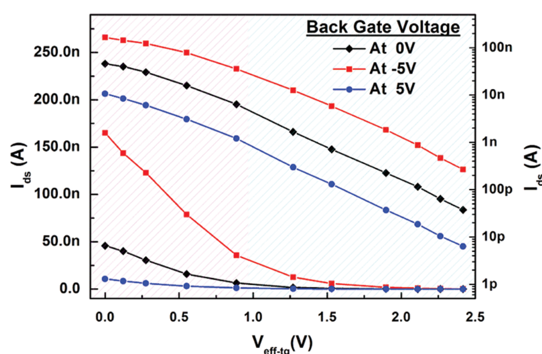

Figure 4. Linear (left axis) and log (right axis) presentations of $I_{ds}-V_{eff\text{-}tg}$ measurements at three constant V_{bgs} (*i.e.*, −5, 0, and 5 V) taken from the $I_{ds}-V_{bgs}$ characteristics of Figure 2.

according to the following relation:[30]

$$\Gamma = \frac{C_{box}}{C_{nox}} = \frac{\ln(\{2d_{nox}+R_{nw}\}/R_{nw})}{\ln(\{2d_{box}+R_{nw}\}/R_{nw})} \quad (1)$$

$$V_{eff\text{-}tg} = \Delta V_{bgs}\cdot\Gamma$$

where C_{nox} and d_{nox} are the capacitance and thickness of Si NW's native oxide, respectively, C_{box} and d_{box} are the capacitance and thickness of the back oxide of the substrate, respectively, and R_{nw} is the radius of the Si NW. Using eq 1, Γ was calculated to be 0.153. This value is similar to the Γ (=0.137) obtained for Si NWs (∼15 nm characteristic dimensions, 400 nm back oxide, and 40 nm top oxide) that was reported elsewhere.[30]

Figure 4 shows the I_{ds} at three constant V_{bgs} (−5, 0, and +5 V) as a function of $V_{eff\text{-}tg}$. Under different decane concentrations (equivalent to 0 V < $V_{eff\text{-}tg}$ < 1 V)—I_{ds} decreased linearly with $V_{eff\text{-}tg}$. At a constant decane concentration (equivalent to $V_{eff\text{-}tg}$ > 1 V), I_{ds} decreased exponentially with $V_{eff\text{-}tg}$ over time. A value of 2.5 V for $V_{eff\text{-}tg}$, which was induced by the decane molecules on

TABLE 2. Calculated Effective Voltage, Interface State Level Density Change, Potential Change at the Bottom of the Si NW, and the Contacts Barrier Height Change

	step (ppm)										
	base	17	43	60	76	76	76	76	76	76	76
time (h) =	0.0	0.5	1.0	1.5	2.0	2.5	3.0	3.5	4.0	4.5	5.0
$\Delta(E_{bnw}D_{nw})$ (V)	0	0	0	0	0	0.003	0.007	0.008	0.009	0.010	0.011
ΔD_{it} (cm^{-2} eV^{-1} $\times$ 10^{10})	0	1.42	3.15	5.31	6.35	6.35	6.35	6.35	6.35	6.35	6.35
$V_{eff\text{-}tg}$ (V)	0	0.12	0.28	0.55	0.89	1.27	1.53	1.90	2.11	2.26	2.42
$\Delta\Psi_b$ (V)	0	0	0.001	0.003	0.019	0.039	0.050	0.059	0.066	0.074	0.078

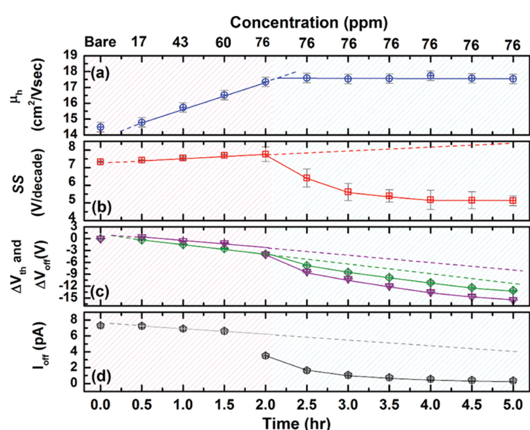

Figure 5. Change of HTS-Si NW FET parameters *versus* decane concentration and exposure time at constant decane concentration (76 ppm). (a) μ_h; (b) SS; (c) V_{th} (◇) and V_{off} (▽); and (d) I_{off}. The point at $t = 0$ h (ref) stands for exposure to reference air.

top of the HTS-Si NW, could be calculated using eq 1; see also Table 2. This result emphasizes that molecular gating is possible not only with polar or ionic analytes[1,16,17] but also with nonpolar ones.

The fundamental parameters of the HTS-Si NW FET during exposure to the analytes were calculated. The threshold voltage (V_{th}) was extracted from the extrapolation to zero of the linear part of the $I_{ds}-V_{bgs}$ characteristics, according to[31,32]

$$I_{ds} = \frac{2\pi\varepsilon_{box}}{\ln(\{2d_{box}+R_{nw}\}/R_{nw})}\mu_h\frac{V_{ds}}{L_{nw}}\left(V_{th} - V_{bgs} + \frac{V_{ds}}{2}\right) \quad (2)$$

where V_{ds} is the source–drain voltage, ε_{box} is the dielectric permittivity of the back oxide of the substrate, and L_{nw} is the length of the (Si NW) channel between the source and drain. The V_{bgs} that characterize the I_{off} (V_{off}) and I_{off} were extracted by fitting the $I_{ds}-V_{bgs}$ curve close to the I_{off} and by calculating the minimum value and its position with this function. Both the shift in V_{th} (ΔV_{th}) and shift in V_{off} (ΔV_{off}) were calculated with respect to the V_{th} and V_{off} of the reference measurement. The hole mobility (μ_h) was extracted from the slope of the linear part of the $I_{ds}-V_{bgs}$ characteristics, using the following relationship:

$$\mu_h = \frac{dI_{ds}}{dV_{bgs}}\frac{\ln(\{2d_{box}+R_{nw}\}/R_{nw})}{2\pi\varepsilon_{box}}\frac{L_{nw}}{V_{ds}} \quad (3)$$

The subthreshold swing (SS), which is the gate voltage necessary to change the I_{ds} by one decade, was extracted in the range of 10^{-10} to 10^{-8} A, using the following relationship:

$$SS = \ln(10)\left(\frac{d\ln(I_{ds})}{dV_{bgs}}\right)^{-1} = \ln(10)\frac{nk_bT}{q} \quad (4)$$

SS was extracted from the slope of the subthreshold logarithm current, according to[31,32]

$$I_{ds} = \frac{2\pi\varepsilon_{box}}{\ln(\{2d_{box}+R_{nw}\}/R_{nw})L_{nw}}\mu_h\left(\frac{nk_bT}{q}\right)^2 \times \exp\left(\frac{q}{nk_bT}\left\{V_{th} - V_{bgs} + \frac{nk_bT}{q}\right\}\right) \quad (5)$$

where k_b is the Boltzmann constant, T is the temperature, n is the ratio of the Si NW capacitance, and q is the elementary charge.

Figure 5 presents the μ_h, SS, V_{th}, V_{off}, and I_{off} extracted at various exposure conditions. As seen in the figure, two regimes were observed. The first regime ($t < 2$ h; marked by pink background) exhibited a linear correlation between the extracted HTS-Si NW FET parameters and the decane concentration. In this regime, increasing the decane concentration (i) increased μ_h linearly (Figure 5a); (ii) shifted V_{th} (rhombus in Figure 5c) and V_{off} (triangles in Figure 5c) linearly to negative back-gate voltages; (iii) increased SS linearly (Figure 5b); and (iv) slightly decreased the I_{off} (Figure 5d). In the second regime ($t > 2$ h; marked by turquoise background), increasing the exposure time on exposure to constant decane concentration (i) kept μ_h constant (Figure 5a); (ii) shifted V_{th} and V_{off} nonlinearly to negative back-gate voltages (Figure 5c); (iii) decreased SS nonlinearly (Figure 5b); and (iv) decreased I_{off} nonlinearly (Figure 5d).

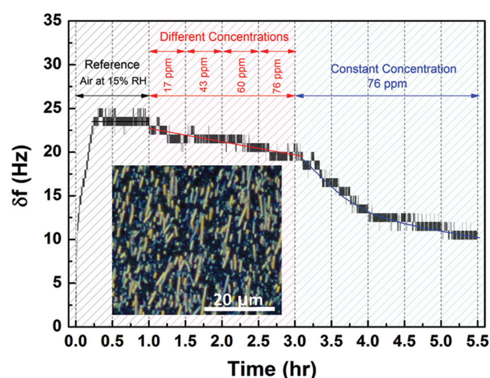

Figure 6. Change in the frequency (δf) of the QCM sensor on exposure to decane during the three sequential exposure steps. Inset: HTS-functionalized Si NW dispersion on a typical gold surface of the QCM sensors that were used to quantify the adsorption kinetics of the nonpolar analytes.

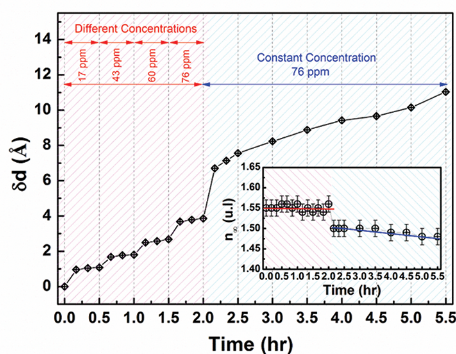

Figure 7. Change of the decane layer thickness (δd) during exposure of HTS-modified planar Si substrate to decane. Inset: The extrapolated electronic part of the refractive index of decane layer (n_∞) during the three sequential exposure steps.

To understand the sensing results of the HTS-Si NW FETs, we investigated the adsorption kinetics and dielectric effect of the decane on the Si NW FET device. We assumed that the analytes are adsorbed on three areas of the HTS-Si NW FET device: (i) the Si NW surface (see Figure 3; Area-A); (ii) the back-oxide surface of the FET device (see Figure 3; Area-B); and (iii) the electrical contacts and/or interface between the Si NW and the metal contact (Area-C).

Effect of Analyte's Adsorption on Area-A. The effect of analyte adsorption on Area-A was investigated with QCM. Figure 6 shows the frequency change (δf) of the QCM resonator (20 MHz) coated with a film of HTS-Si NWs upon exposure to reference air and to decane (*see* Figure 6, inset). The Sauerbrey's equation relates δf (in Hz) to the mass change (Δm; in ng):

$$\Delta m = -C_f A\, \delta f \qquad (6)$$

where C_f is the mass sensitivity (=1.104 ng cm^{-2} Hz^{-1}) and A is the active area of the QCM resonator (=0.2 cm^2). To evaluate the mass upload on an individual HTS-Si NW, the calculated Δm was normalized by the effective area ($A_{eff} = \Sigma_1^n 2\pi R_{nw} L_{nw}$, wherein n is the number of the HTS-Si NWs on the QCM resonator) of all Si NWs on the QCM resonator.[33] As seen in Figure 6, δf increased on exposure to the reference air, reaching a saturation level after 0.5 h. The increase in δf could be attributed to the removal of solvent residues (*i.e.*, the 2-propanol used for the suspension of the Si NWs) and/or water molecules from the Si NW surface. Exposure to decane decreased δf, compared to the reference level. At different concentrations (1 h < t < 3 h), each partial change caused a linear change in δf, indicating a linear accumulation of decane at the surface of the HTS-Si NWs. Extended periods of exposure to 76 ppm decane (t > 3 h) led to a nonlinear decrease in δf, implying an incremental accumulation of decane on the HTS-Si NWs. Similar quantitative observations were obtained upon exposure to hexane and octane (not shown). In a complementary test (not shown), a bare (Si NW-free) QCM resonator showed negligible response to decane exposure (0 ± 1 Hz).

On the basis of the data shown in Figure 6, the thickness of the analyte layer (d_{mol}) on the Si NW surface (see Figure 3, Area-A) was evaluated by

$$d_{mol} = \frac{\Delta m}{\rho A_{eff}} \qquad (7)$$

where ρ stands for the analyte liquid density. Our calculations showed that a change of 1 Hz in δf is equivalent to a formation of a ~3 ± 1 nm thick film of decane on each individual HTS-Si NW. On the basis of eq 7, the adsorbed decane thickness is ~9 ± 3 nm at t = 3 h and ~45 ± 15 nm at t = 5.5 h.

Effect of Analyte Adsorption on Area-B. The thickness evaluated by QCM does not give any implication regarding the adsorption of decane of the planar (Si NW-free) surface of the device (*cf.* Area-B in Figure 3 and footnote 33). To evaluate the thickness of the adsorbed decane layer on the back oxide of the FET, HTS-modified *planar* Si(111) substrates with a native oxide layer were examined by *in situ* spectroscopic ellipsometry.[35] As seen in Figure 7, exposure to decane increased the decane layer thickness (δd), compared to the reference level. At 0 h < t < 2 h, each differential change in the decane concentration caused a step-like trend of δd. For a given concentration, the thickness increased during the first 15 min of exposure, but reached a saturation value afterward. Extended periods of exposure to 76 ppm of decane (t > 2 h) led to a nonlinear increase in δd, implying an incremental accumulation of decane on the HTS-Si surface. Similar quantitative observations were obtained on exposure to hexane and octane (not shown).

The electronic part of the refractive index, n_∞, was extrapolated from the wavelength-dependent

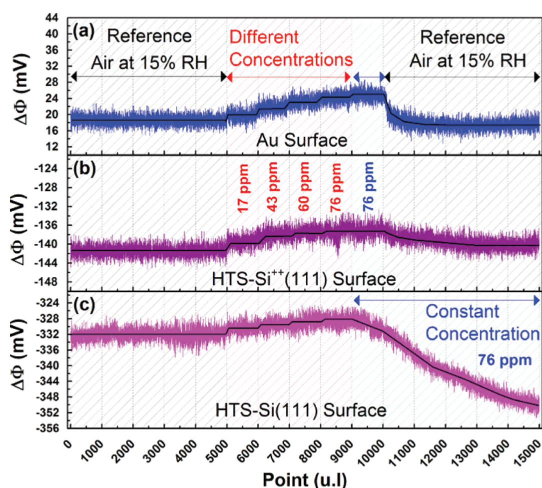

Figure 8. Change of the work function ($\Delta\Phi$) during exposure of (a) Au surface; (b) HTS-modified planar highly doped Si substrate (HTS-Si^{++}(111)); and (c) HTS-modified planar low-doped Si substrate (HTS-Si(111)), during the three sequential exposure steps. The Φ of Au, HTS-Si^{++}(111), and HTS-Si(111) under reference air was measured to be 5.118 $\pm$ 0.02, 4.958 $\pm$ 0.02, and 4.768 $\pm$ 0.02 eV, respectively.

refractive index, $n(\lambda)$, in the UV-NIR spectral region and squared to obtain the layer's low-frequency dielectric constant ($k_{nonpolar}$):

$$k_{nonpolar} = (\lim_{\lambda \to \infty} \{n(\lambda)\})^2 = n_\infty^2 \qquad (8)$$

where λ is the wavelength. The electronic part of the refractive index of the HTS layer (n_{HTS}) was found to be dispersion-free and almost absorption-free between 670 and 1800 nm, at a value of n_{HTS} = 2.10 $\pm$ 0.05. At different concentrations (0 h < t < 2 h), the electronic part of the refractive index of decane (n_{decane}) was found to be n_{decane} = 1.55 $\pm$ 0.02, as seen in the inset of Figure 7. During extended periods of exposure to 76 ppm decane (t > 2 h), n_{decane} was found to decrease slightly from 1.50 $\pm$ 0.02 to 1.48 $\pm$ 0.02. Similar values of n_∞ were obtained upon exposure to hexane and octane (not shown). On the basis of these results, the adsorbed decane thickness is ~0.40 $\pm$ 0.01 nm at t = 2 h and ~1.10 $\pm$ 0.01 nm at t = 5.5 h.

Effect of Analyte Adsorption on Area-C. For Area-C, it is well known that a Schottky (barrier) contact is formed when the Ti/Au metal layer is directly connected to a low-doped p-type Si.[36,37] When this contact is used in a Si NW FET sensor, the barrier might change considerably even with minute adsorption of gaseous analytes.[36,37] This could be a result of a change in the work function (Φ) of the metal and/or the semiconductor parts of the contact.

To understand the contribution of Area-C to the sensing results of the HTS-Si NW FETs, the changes of work function ($\Delta\Phi$) of Au and of the contact-free p-type Si(111) before and after exposure to analytes were investigated. Figure 8a and b show the $\Delta\Phi$ of Au and highly doped (0.008–0.02Ω· cm, ~10^{-19} cm^{-3}) n-type HTS-Si(111)—(hereon, HTS-Si^{++}(111))—surface on exposure to reference air and to noninteracting, nonpolar decane under 15% RH. As seen in the figures, the maximum $\Delta\Phi$ obtained during the exposure of Au or HTS-Si^{++}(111) to decane was *ca.* 4 meV. For both the Au and the HTS-Si(111) surfaces, the $\Delta\Phi$ remained constant for a long period under high concentrations (76 ppm) (shown only for the first 0.5 h in Figure 8a and b) and was restored upon cleaning the surfaces with reference air. Figure 8c shows the $\Delta\Phi$ of low-doped (9–16 Ω·cm, ~10^{-15} cm^{-3}) p-type HTS-Si(111)—here on HTS-Si(111). The maximum $\Delta\Phi$ obtained during the exposure of HTS-Si^{++} (111) to decane was *ca.* 4 meV. However, for a long period under the higher concentration (*i.e.*, 76 ppm), the $\Delta\Phi$ decreased significantly, by *ca.* 20 mV.

In a complementary study to understand the contribution of Area-C to the sensing results of the HTS-Si NW FETs, the contacts of the HTS-Si NW FET were passivated with poly(methyl methacrylate) (PMMA); see Supporting Information, Figure 3S. On exposure to analytes, the PMMA-passivated HTS-Si NW FET showed the same trends in the $I_{ds}-V_{bgs}$ characteristics as the unpassivated HTS-Si NW FET (see Supporting Information, Figure 3S). Exceptions were the shifts and the decrease in I_{off}, which exhibited less pronounced changes under extended exposure to 75 ppm decane, most probably because the contact is already dielectrically affected from the PMMA passivation (k_{PMMA} = 2.6).

DISCUSSION

The results of the QCM measurements (Figure 6) are consistent with the results of the SE measurements (Figure 7). The lower the δf obtained by the QCM, the higher the δd obtained by SE. Comparison between the different regimes in Figures 5–7 shows a good correlation between the electrical characteristics of the HTS-Si NW FETs (Figure 5) and the adsorption kinetics of decane (Figures 6 and 7). The two regimes observed in Figures 4–7 indicate two sensing mechanisms. The first mechanism is based on the effect of charged surface states, whereby adsorption of analyte molecules in between or on top of the chains and/or in the pinholes of the adsorptive monolayer molecules changes the charged surface states at the SiO_2/monolayer interface (*cf.* ref 2 for more details). The second mechanism was associated with a molecular gating due to dielectric changes in the environment proximate to the Si NW surface (*cf.* Area-A in Figure 3 and refs 38–40). This is supported by the SE analysis (Figure 7), assuming that the same dielectric changes that occur at the planar HTS-Si(111) surface (*cf.* Figure 3; Area-B) occur also at the Si NW surface. Under this assumption, the dielectric environment in close proximity to the Si NW surface was changed from air,

characterized by k_{air}= 1, to a decane nanolayer, characterized by $k_{decane} \approx 2.2$, during the exposure process. The sudden decrease in n_{decane} at t = 2 h (see inset of Figure 7) indicates a transition between different mechanisms. The moderate decrease of n_{decane} at extended periods of exposure (t > 2 h) might be an indication of the formation of multilayers of absorbed decane molecules. In this case, the moderate decrease in n_{decane} that has led to $n_{decane} \approx 1.48 \pm 0.02$ (at t = 5.5 h) indicates values that are close to the n_{decane} of liquid decane ($n_{l\text{-}decane}$ = 1.41).[41] In other words, the changes in n_{decane} indicate a transition from interface to bulk properties of the decane layer that was adsorbed on the Si NW surface. In the following sections, we use a model-supported analysis to discuss the effect of the molecular gating on the fundamental features of the Si NW FET, in regard to the "charged surface states effect" and the "dielectric effect" sensing mechanisms.

Carrier Mobility. Generally, μ_h of the Si NW FET can be described by the following relationship:[29]

$$\mu_h = \frac{\mu_0}{1 + \left|\frac{1}{\varepsilon_{si}E_0}\left(Q_D + \frac{Q_S}{\eta}\right)\right|^{\gamma}} \quad (9)$$

where Q_D is the depletion charge density, Q_S is the mobile charge density, μ_o is the low field mobility (the mobility in the absence of gate applied field), ε_{si} is the silicon permittivity, and γ, η, and E_0 are empirical parameters. Under strong carrier accumulation (above V_{th}) $Q_D \ll Q_S$.[42] Assuming $\gamma = 1$[29] for Si NW, the change in μ_h (*i.e.*, $\Delta\mu_h$) because of a small change in Q_S (*i.e.*, ΔQ_S) is

$$\Delta\mu_h \approx -\Delta Q_S \frac{\dfrac{\mu_0}{\varepsilon_{si}E_0\eta}}{\left(1 + \dfrac{Q_S{}^0}{\varepsilon_{si}E_0\eta}\right)^2} \quad (10)$$

where $Q_s{}^0$ is Q_s of the Si NW under reference air. According to eq 10, a decrease in the total density of hole carriers (ΔQ_S < 0), as a response to the decrease in the negatively charged surface state density (*cf.* ref 2 for more details), leads to a linear increase in μ_h (*cf.* refs 2 and 43). This process saturates when the maximum change in the negatively charged surface states is reached. From this point on, μ_h remains constant, irrespective of any change in the dielectric properties of the layer surrounding the Si NW. These results indicate that μ_h could be used to characterize the molecular gating of nonpolar analytes at low concentrations, due to the charged surface state effect. In contrast, μ_h cannot be used for the characterization of nonpolar analytes at high/constant concentrations for extended periods or due to changes in the dielectric medium.

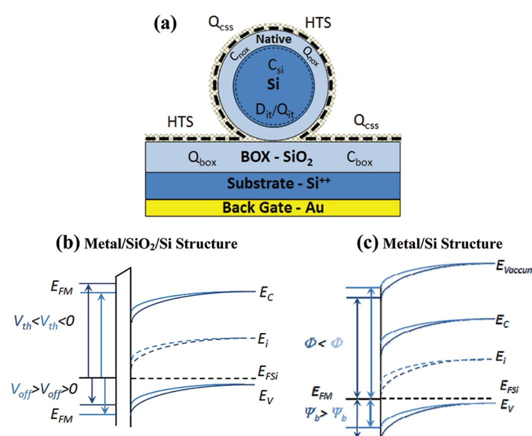

Figure 9. (a) Cross-section schematics of the HTS-Si NW FET. (b) Energy band diagram of the Au/Si^{2+}/BOX-SiO_2/Si capacitor structure, along the radius of the bottom Si NW, before and after an increase in E_{bnw}. (c) Energy band diagram along the source or drain Au/Ti/Si contacts before and after an increase in E_{bnw}. The bottom of the Si NW is defined as the closest (oxide-free) Si point to the BOX-SiO_2. E_C, E_V, C_{FSi}, E_{vacuum}, and E_i stand for the conductive, valence, Fermi, vacuum, and intrinsic Fermi energies of the Si NW, respectively, and E_{FM} is the Fermi energy of the gate, source, and drain (metal) material.

Subthreshold Swing. The subthreshold swing (SS) is given by the following expression:

$$SS = \ln(10)\left(\frac{q}{k_bT} - \frac{1}{E_{bnw}D_{nw}}\right)^{-1}\left(1 + \frac{C_{it}}{C_{box}} + \frac{C_{si}}{C_{box}}\right) \quad (11)$$

where E_{bnw} is the field at the bottom of the Si NW (the closest oxide-free Si point to the BOX-SiO_2; *cf.* Figure 9), D_{nw} is the Si NW diameter, C_{box} is the back oxide capacitance, C_{si} is the capacitance of the Si NW, and C_{it} is the capacitance of interface states at the Si/SiO_2 region of the Si NW. The linear increase in SS in Figure 5 (when t < 2 h) can be demonstrated by a linear change in C_{it} (*i.e.*, ΔC_{it}) according to

$$\Delta C_{it} = \frac{C_{box}}{\beta}(SS - SS^0) \quad (12)$$

$$\beta = \ln(10)\left(\frac{q}{k_bT} - \frac{1}{E^0_{bnw}D_{nw}}\right)^{-1}$$

where E^0_{bnw} is the field at the bottom of the Si NW under reference air and SS^0 is the SS under reference air. ΔC_{it} arises from a change in the interface-state density (D_{it})[44] according to $\Delta C_{it} = q^2 \Delta D_{it}$.[37] According to our calculations, a linear change of $\sim 6 \times 10^{10}$ cm^{-2} eV^{-1} in D_{it} gives rise to the observed changes in SS (*ca.* 0.4 V/decade between t = 0–2 h); *cf.* Table 2. This change in D_{it} is significantly smaller than D_{it} of the native silicon oxide (1×10^{12} cm^{-2} eV^{-1}).[37] Therefore, it is reasonable to assume that a change in the configuration of the HTS molecules, due to adsorption of nonpolar analytes,[2] could induce a small (<5%) change in D_{it}.

The nonlinear decrease in SS (*i.e.*, $t > 2$ h) can be estimated according to

$$\Delta E_{\mathrm{bnw}} = \frac{\frac{\alpha}{D_{\mathrm{nw}}}\left(\frac{k_{\mathrm{b}}T}{q}\right)^2(\mathrm{SS}^{\mathrm{high}} - \mathrm{SS})}{\left(\mathrm{SS} - \alpha\frac{k_{\mathrm{b}}T}{q}\right)\left(\mathrm{SS}^{\mathrm{high}} - \alpha\frac{k_{\mathrm{b}}T}{q}\right)} \qquad (13)$$

$$\alpha = \ln(10)\left(1 + \frac{C_{\mathrm{it}}^{\mathrm{high}}}{C_{\mathrm{box}}} + \frac{C_{\mathrm{si}}}{C_{\mathrm{box}}}\right)$$

where $C_{\mathrm{it}}^{\mathrm{high}}$ is the C_{it} at $t = 2$ h and $\mathrm{SS}^{\mathrm{high}}$ is the SS at $t = 2$ h. Our calculations show that a nonlinear change of *ca.* 0.0103 V in $E_{\mathrm{bnw}}D_{\mathrm{nw}}$ gave rise to the observed changes in SS (*ca.* 2.6 V/decade); see Table 2. This change in $E_{\mathrm{bnw}}D_{\mathrm{nw}}$ is comparable to the thermal voltage ($k_{\mathrm{b}}T/q = 0.0260$ V), meaning significant band bending inside the Si NW. The band bending inside the Si NW is discussed below.

These results indicate that SS is a good parameter to characterize the "molecular gating" of a nonpolar analyte, both at low concentrations and high/constant concentrations for extended exposure periods. Furthermore, the sign and magnitude of ΔSS could be used to determine the type of sensing mechanism controlling the molecular gating. A positive, small change in ΔSS could be an indication of the charged surface state effect, while a large, negative change in ΔSS could be an indication of the dielectric effect.

Threshold Voltage. V_{th} for an accumulation–conduction FET is understood as the V_{bgs} value that corresponds to the onset of significant I_{ds}. At this V_{bgs} the bottom Si NW surface potential is essentially zero (flat band)[37] and V_{th} is given by the following equation:

$$V_{\mathrm{th}} = V_{\mathrm{FB}} - \frac{Q_{\mathrm{box}}}{C_{\mathrm{box}}} - \frac{Q_{\mathrm{D}}}{C_{\mathrm{box}}} \qquad (14)$$

where V_{FB} is the difference between the work function of the gate material and the Si NW, Q_{box} is the sum of all (fixed and trapped) charges in the back oxide of the substrate, including the negative charged surface state at the molecule/back SiO_2 interface (Q_{css}), and Q_{D} is the absolute charge at the Si NW depletion layer. According to this relationship, ΔV_{th} is given by the following expression:

$$\Delta V_{\mathrm{th}} \approx \frac{\Delta Q_{\mathrm{css}}}{C_{\mathrm{box}}} - \frac{\Delta Q_{\mathrm{d}}\{\Delta Q_{\mathrm{it}}, \Delta E_{\mathrm{bnw}}, \Delta Q_{\mathrm{css}}\}}{C_{\mathrm{box}}} \qquad (15)$$

Assuming that ΔQ_{css} everywhere on the SiO_2 surface of the Si NW FET (*cf.* Figure 9) is nearly balanced by a mirror image charge,[45] this would lead to a change in the channel conductivity, but also to a shift in the V_{th}. In other words, a change in Q_{css} everywhere on the oxide surface of the Si NW FET might change Q_{D} considerably (second-order change) (*cf.* also refs 46 and 21). Nevertheless, a decrease in Q_{css} ($\Delta Q_{\mathrm{css}} < 0$) gave rise to the observed negative shift of V_{th} ($\Delta V_{\mathrm{th}} < 0$) at $t < 2$ h.

Relation between E_{bnw} and ΔV_{th} and ΔV_{off}. The question of how the change in E_{bnw} relates to ΔV_{th} and ΔV_{off} remains. To answer this question, the operation principle of an accumulation–conduction p-type FET device must first be considered. When a large negative voltage (above the V_{th}) is applied to the back gate of a p-type FET, an excess of holes is induced at the bottom of the Si NW (*cf.* Figure 9).[37] In this case, the bands close to the bottom of the Si NW are bent upward (see Figure 9). Applying a back gate voltage below V_{th} leads to a downward bending and to a depletion of the holes until full depletion of the Si NW occurs (depletion region). Between these two occurrences, the depletion layer inside the Si NW increases.[37] The higher the depletion layer, the higher the band bending, and the higher the Q_{D}. When a large positive voltage is applied to the back gate, the bands bend downward even more until excess electrons start to be induced at the bottom of the Si NW (weak inversion region).[37] The back gate voltage that separates the depletion region and the weak inversion region, apparent in the I_{ds}–V_{bgs} characteristics, is termed V_{off}. With this in mind, a change in E_{bnw} should be expressed both in the V_{th} and the V_{off} positions, as schematically represented in Figure 9b. As seen in the figure, the higher the E_{bnw}, the higher the value of V_{th} (negative) that is needed to reach the accumulation mode. Additionally, the higher E_{bnw} the lower the value of V_{off} (positive) that is needed to reach the weak inversion mode. It is worth pointing out that ΔV_{th} and ΔV_{off} are of the same order of magnitude and follow similar trends (*cf.* Figure 5c). Interestingly, ΔV_{off} of decane at $t = 2$ h deviates from the linear fit for the points at $t < 2$ h, implying that a change of the sensing mechanism started to take place. The deviation of the QCM's δf at a similar transition point from the linear fit of the points at $t < 2$ h supports this claim. These results indicate that the combination of ΔV_{off} and ΔV_{th} could be used to characterize the two sensing mechanisms, as well as the transition between them.

Off-Current. To determine the relation between E_{bnw} and I_{off}, the operation principle of metal/p-type semiconductor contact should first be considered. It is well known that a Schottky barrier is formed when the Au/Ti layer metal is in direct contact with low-doped p-type Si.[36,37] This contact is strongly influenced by the V_{bgs}. At high negative V_{bgs}, where the device turns to on-state, the holes may tunnel through the barrier. This is because the width of the contact barrier decreases; namely, the barrier height no longer limits the current flow through the Si NW.[36,37] At high positive V_{bgs}, particularly at V_{off}, where the device turns to the off-state, the I_{sd} is governed by diffusion and is limited by the barrier height of the contact.[36,37] With this in mind, a change in E_{bnw} should be expressed also in the barrier height, Ψ_{b}, of the contacts, as schematically represented in Figure 9c. As seen in the figure, the higher the

band bending, the higher the Ψ_b and the lower the I_{off} (*cf.* Figure 2b). At the same time, at high negative V_{bgs} the I_{sd} are not influenced by Ψ_b, and therefore, the mobility remains constant although E_{bnw} is changed dramatically. The observation of constant I_{off} under exposure to the different concentrations, at $t < 2$ h, indicates that the Ψ_b was not changed because of ΔQ_{css}.

To express the effect of I_{off} (the Schottky emission current) quantitatively, the following relationship is considered:

$$I_{off} \propto \exp\left(-\frac{q\Psi_b}{k_b T}\right) \quad (16)$$

According to this relationship, $\Delta\Psi_b$ is given by the following expression:

$$\Delta\Psi_b = -\frac{k_b T}{q}\ln\left(\frac{I_{off}}{I_{off}^0}\right) \quad (17)$$

where I_{off}^0 is I_{off} of the Si NW under reference air. Our calculations show that a nonlinear change of *ca.* 0.078 V in Ψ_b gave rise to the observed changes in I_{off}; see Table 2. This change in Ψ_b is *ca.* 9% of the Au/Ti/Si barrier height (0.84 eV),[36] meaning significant band bending inside the Si NW. The KP result (Figure 8) shows that neither the work function of Au nor the work function of Si was changed (see Figure 8a and b) at low concentrations (at $t < 2$ h), indicating that Ψ_b is constant and $\Delta\Psi_b \approx 0$. For a long period under the higher concentration (at $t > 2$ h), Ψ_b is changed because of a change in the Si NW band bending. This result is consistent with the decrease of Φ of HTS-Si(111); *cf.* Figure 8 and Figure 9c. Interestingly, I_{off} and $\Delta\Psi_b$ of decane at $t = 2$h, as the case of ΔV_{off}, deviated from the linear fit for the points at $t < 2$ h. These results indicate that I_{off} could be used to characterize the two sensing mechanisms, as well as the transition between them.

SUMMARY AND CONCLUSIONS

We have presented experimental evidence for detection of nonpolar species with Si NW FETs and presented a model to explain the results. According to the model, the sensing of nonpolar analytes could be ascribed to molecular gating, due to two *indirect* effects. The first effect was attributed to changes in the charged surface states, mostly due to analyte-induced conformational changes in the organic monolayer that affect the density of charged surface states at the SiO_2/monolayer interface. The second effect was attributed to changes in the dielectric medium (or condensed analytes) close to the Si NW surface. These effects are manifested in the changes of the fundamental parameters of the Si NW FET (μ_h, V_{th}, I_{off}, V_{off}, and SS). Model-based analysis indicated that μ_h is appropriate to characterize the molecular gating of nonpolar analytes at low concentrations, but cannot be used for the characterization of nonpolar analytes at high/constant concentrations for extended periods. The SS was found to be appropriate for expressing the molecular gating of nonpolar analytes, at both low concentrations and high/constant concentrations for extended exposure periods. Finally, a combination of ΔV_{off} and ΔV_{th} with ΔI_{off} was found to be most appropriate for expressing the effects of surface states and dielectric medium and the transition between them. The detection of nonpolar species in real confounding environments with high and fluctuating levels of humidity as well as "fouling" nonspecific binding is a major step toward the realization of real-world applications that do not yet use Si NW FETs for environmental monitoring, homeland security, food quality control, or medicine.

METHODS

Synthesis and Functionalization of Si NWs. The synthesis of the Si NWs[47] as well as the fabrication of Si NW FETs was described earlier.[2] Briefly, Si NWs were prepared by the vapor−liquid−solid growth technique, yielding p-type (112) Si NWs doped with boron to a doping level of $\sim 10^{16}$ cm^{-3}. Transmission electron microscopy data indicated that these Si NWs consisted almost entirely of smooth Si cores (50 ± 5 nm in diameter) coated with a $\sim 5 \pm 1$ nm native SiO_2 layer (see Figure 1b, inset).

Functionalization of Si NWs. The Si NWs were functionalized with a stable 0% cross-linked hexyltrichlorosilane monolayer using the two-step amine-promoted reaction procedure described elsewhere.[24,48,49] This monolayer was shown to passivate a majority of oxide surface states and to result in stable hysteresis-free, reproducible characteristics upon exposure to analytes.

Si NW FET Measurements. The FET devices used in the current study consist of an individual Si NW between source and drain Au/Ti electrodes (10 nm Ti and 100 nm Au) that are mutually separated by 2 μm on top of a 100 nm thermally oxidized degenerately doped p-Si (0.001Ω·cm resistivity) substrate (see Figure 1 and ref 2 for more details). Some of the devices were passivated with a 200 nm poly(methyl methacrylate) layer that covered 300 nm of the Si side of the Au/Si NW contacts and all of the Au contact area, except a rectangular area for the electrical probe contacting (see Supporting Information, Figures 3S). A probe station that is connected to a device analyzer (Agilent B1500A) was used to collect the electrical signals of the Si NW FETs before and/or after exposure to analytes. Source−drain current (I_{ds}) *versus* voltage-dependent back-gate (V_{bgs}) measurements, swept backward between +40 V and −40 V with 200 mV steps and at 1 V source−drain voltage (V_{ds}), were used to determine the performance of Si NW FET sensors.[2]

Quartz Crystal Microbalance Measurements. A suspension HTS-Si NWs in 2-propanol was delivered to a gold-coated quartz crystal microbalance resonator (5 mm in diameter; 20 MHz) and dried with pure air (<0.3 ppm organic contaminants); see inset of Figure 6. The QCM resonator was then placed in a vacuum oven at 80 °C for 12 h to eliminate 2-propanol residues. A clean QCM resonator without HTS-Si NWs was used as reference sample. Frequency shifts (δf), before and after exposure to analytes, were recorded by LibraNose 2.1 (Technobiochip, Elba Island, Italy), a system that is composed of a measurement chamber with eight QCM sensors, an internal micropump, a microelectric

valve that conveys the gas sample (with an average flow of 0.1 L·min^{-1}) to the measuring chamber, and the electronic part.

Ellipsometry Measurements. The dielectric properties and thickness of the adsorbed overlayer that formed during the exposure to nonpolar analytes were determined *in situ* by spectroscopic ellipsometry. For this purpose, planar Si(111) substrates having 1.7 ± 0.3 nm native oxide were coated with HTS in the same way as the Si NWs. A variable-angle rotating compensator spectroscopic ellipsometer (M-2000 V, J. A. Woollam Co., Inc.) was equipped with a specially designed triangular exposure cell that allowed *in situ* measurements at an angle of incidence of 70°. Vapor of nonpolar analytes was supplied via a flow system similar to the one connected to the exposure chamber for the QCM measurements (with an average flow of 0.5 L·min^{-1}). The ellipsometric angles were recorded over a spectral range of 250−1700 nm, and a four-phase nonpolar analyte/HTS/native SiO_2/Si substrate model was used to extract the electronic contribution to the refractive index, *n*, and the thickness of the adsorbed nonpolar layer. The exact thickness of the native oxide layer was determined through SE measurements at five incidence angles (60°, 65°, 70°, 75°, 80°) on an open sample stage, prior to the HTS functionalization, using tabulated values for the refractive indices of Si and SiO_2.[50,51] The thickness and refractive index of the HTS layer were also determined from multiangle SE measurements on the open sample stage. Absorption-free Cauchy dispersion was assumed for the absorbed nonpolar layer, since the refractive index of the nonpolar analytes in solution also follows Cauchy dispersion.

Kelvin Probe Measurements. The work function change ($\Delta\Phi$) of Au and the HTS-Si surfaces as a result of the adsorbed overlayer that formed during the exposure to nonpolar analytes was determined *in situ* by Kelvin probe. For this purpose, planar highly doped (0.008−0.02 Ω· cm) Si(111) substrates having 1.7 ± 0.3 nm native oxide were coated with HTS in the same way as the Si NWs, and a standard Al sample coated with 100 nm Au layer was used with an ambient Kelvin probe package from KP Technology Ltd. (U.K.). This KP package includes a head unit with an integral tip amplifier, a 2 mm tip, a PCI data acquisition system, a digital electronics module, the system software, an optical baseboard with sample and Kelvin probe mounts, and a 1 in. manual translator, all placed inside a Faraday cage. The work function resolution of the system is 1−3 mV. The Kelvin probe technique measures the contact potential difference (CPD) between a vibrating reference Au probe and the sample (Φ_{Au} = 5.1 eV). The CPD is defined as the difference in the work function of the two surfaces. For metal and highly doped Si surfaces, where band bending effects are negligible, a CPD measurement yields the difference in electron affinity (χ). For low-doped Si surfaces, the CPD is a sum of the electron affinity change and the surface band bending change. Typically, the CPD is extracted after a saturation of 500 measurements points (*ca.* 15 min). However, for the sake of detecting small changes of nonpolar analytes with maximum precision and high signal-to-noise ratio, the CPD was extracted after a saturation of 5000 measurements points (*ca.* 2.5 h). The measurement's deviation is ±20 mV.

Exposure to Analytes. The signals of the QCM and Si NW FET samples were monitored during three sequential steps: (i) exposure to a reference air (15% relative humidity (RH) and <0.3 ppm organic contaminants); (ii) exposure to a series of nonpolar analytes (hexane, octane, and decane; see Table 1) that are diluted in the reference air; and (iii) exposure to analytes at high constant concentration for extended periods. The control over the analyte concentration was obtained by passing the reference air (with an average flow of 5 L min^{-1}) through a glass bubbler containing a liquid phase of the analyte of interest (purchased from Sigma Aldrich Ltd. and Fluka Ltd.; >99% purity; <0.001% water). The air emitted from the bubblers, mostly under saturation conditions, was diluted (with an average total flow of 5 L min^{-1}) with the reference air to reach lower levels of analyte concentrations. This way, the system was able to regulate the analyte concentration levels between 1 and 200 ppm. The concentration levels of analytes were measured by a commercial photoionization detector (ppbRAE 3000; Rae Systems, USA) with a detection limit of ~10 ppb.

Acknowledgment. The research leading to these results has received funding from the FP7-Health Program under the LCAOS (grant agreement no. 258868). We acknowledge Nadav Bachar and Rawi Dirawi (Technion) for technical assistance. H.H. is a Knight of the Order of Academic Palms.

Supporting Information Available: Linear-scale (left axis) and log-scale (right axis) presentations of shifted $I_{ds}-V_{bgs}$ measurements under various exposure conditions. Optical images of representative PMMA-passivated Si NW FET device. $I_{ds}-V_{bgs}$ measurements of PMMA-passivated HTS-Si NW FET sensor under various exposure conditions. This material is available free of charge *via* the Internet at http://pubs.acs.org.

Note Added after ASAP Publication: This paper was published on December 23, 2011 with an error in eq 6. The corrected version was reposted on December 30, 2011.

REFERENCES AND NOTES

1. Tisch, U.; Haick, H. Nanomaterials for Cross-Reactive Sensor Arrays. *MRS Bull.* **2010**, *35*, 797–803.
2. Paska, Y.; Stelzner, T.; Christiansen, S.; Haick, H. Enhanced Sensing of Nonpolar Volatile Organic Compounds by Silicon Nanowire Field Effect Transistors. *ACS Nano* **2011**, *5*, 5620–5626.
3. McAlpine, M. C.; Ahmad, H.; Wang, D.; Heath, J. R. Highly Ordered Nanowire Arrays on Plastic Substrates for Ultrasensitive Flexible Chemical Sensors. *Nat. Mater.* **2007**, *6*, 379–384.
4. Stern, E.; Vacic, A.; Reed, M. A. Semiconducting Nanowire Field-Effect Transistor Biomolecular Sensors. *IEEE Trans. Electron Devices* **2008**, *55*, 3119–3130.
5. Li, Y.; Qian, F.; Xiang, J.; Lieber, C. M. Nanowire Electronic and Optoelectronic Devices. *Mater. Today* **2006**, *9*, 18–27.
6. Patolsky, F.; Lieber, C. M. Nanowire Nanosensors. *Mater. Today* **2005**, *8*, 20–28.
7. Patolsky, F.; Zheng, G.; Hayden, O.; Lakadamyali, M.; Zhuang, X.; Lieber, C. M. Electrical Detection of Single Viruses. *Proc. Natl. Acad. Sci.* **2004**, *101*, 14017–14022.
8. Cui, Y.; Wei, Q.; Park, H.; Lieber, C. M. Nanowire Nanosensors for Highly Sensitive and Selective Detection of Biological and Chemical Species. *Science* **2001**, *293*, 1289–1292.
9. Sysoev, V. V.; Button, B. K.; Wepsiec, K.; Dmitriev, S.; Kolmakov, A. Toward the Nanoscopic “Electronic Nose”: Hydrogen *vs* Carbon Monoxide Discrimination with an Array of Individual Metal Oxide Nano- and Mesowire Sensors. *Nano Lett.* **2006**, *6*, 1584–1588.
10. Meier, D. C.; Semancik, S.; Button, B.; Strelcov, E.; Kolmakov, A. Coupling Nanowire Chemiresistors with MEMS Microhotplate Gas Sensing Platforms. *Appl. Phys. Lett.* **2007**, *91*, 063118/1–063118/3.
11. Gao, X. P. A; Zheng, G.; Lieber, C. M. Subthreshold Regime Has the Optimal Sensitivity for Nanowire FET Biosensors. *Nano Lett.* **2010**, *10*, 547–552.
12. Puniredd, S. R.; Assad, O.; Stelzner, T.; Christiansen, S.; Haick, H. Catalyst-Free Functionalization for Versatile Modification of Nonoxidized Silicon Structures. *Langmuir* **2011**, *27*, 4764–4771.
13. Assad, O.; Puniredd, S. R.; Stelzner, T.; Christiansen, S.; Haick, H. Stable Scaffolds for Reacting Si Nanowires with Further Organic Functionalities while Preserving Si-C Passivation of Surface Sites. *J. Am. Chem. Soc.* **2008**, *130*, 17670–17671.
14. Bashouti, M. Y.; Tung, R. T.; Haick, H. Tuning Electrical Properties of Si Nanowire Field Effect Transistors by Molecular Engineering. *Small* **2009**, *5*, 2761–2769.
15. Bashouti, M. Y.; Stelzner, T.; Berger, A.; Christiansen, S.; Haick, H. Covalent Attachment of Alkyl Functionality to 50 nm Silicon Nanowires through Chlorination/Alkylation Process. *J. Phys. Chem. C* **2009**, *113*, 14823–14828.
16. Ramgir, N. S.; Yang, Y.; Zacharias, M. N. Nanowire-Based Sensors. *Small* **2010**, *6*, 1705–1722.
17. He, B.; Morrow, T. J.; Keating, C. D. Nanowire Sensors for Multiplexed Detection of Biomolecules. *Curr. Opin. Chem. Biol.* **2008**, *12*, 522–528.

18. He, T.; Corley, D. A.; Lu, M.; Di Spigna, N. H.; He, J.; Nackashi, D. P.; Franzon, P. D.; Tour, J. M. Controllable Molecular Modulation of Conductivity in Silicon-Based Devices. *J. Am. Chem. Soc.* **2009**, *131*, 10023–10030.
19. Dubey, G.; Rosei, F.; Lopinski, G. P. Modulation of Flat-Band Voltage on H-Terminated Silicon-on-Insulator Pseudo-Metal-Oxide-Semiconductor Field Effect Transistors by Adsorption and Reaction Events. *J. Appl. Phys.* **2011**, *109*, 104904/1–104904/7.
20. Takulapalli, B. R. Molecular Sensing Using Monolayer Floating Gate, Fully Depleted SOI MOSFET Acting as an Exponential Transducer. *ACS Nano* **2010**, *4*, 999–1011.
21. Hovel, H. J. Si Dilm Electrical Characterization in SOI Substrates by the HgFET Technique. *Solid-State Electron.* **2003**, *47*, 1311–1333.
22. Natan, A.; Kronik, L.; Haick, H.; Tung, R. T. Electrostatic Properties of Ideal and Non-Ideal Polar Organic Monolayers: Implications for Electronic Devices. *Adv. Mater.* **2007**, *19*, 4103–4117.
23. Landheer, D.; Aers, G.; McKinnon, W. R.; Deen, M. J.; Ranuarez, J. C. Model for the Field Effect from Layers of Biological Macromolecules on the Gates of Metal-Oxide-Semiconductor Transistors. *Appl. Phys. Lett.* **2005**, *98*, 044701.
24. Paska, Y.; Haick, H. Controlling Properties of Field Effect Transistors by Intermolecular Cross-linking of Molecular Dipoles. *Appl. Phys. Lett.* **2009**, *95*, 233103/1–233103/3.
25. Nonpolar analytes, unlike the polar ones, have negligible chemical or physical interaction with water molecules present in a humid atmosphere.
26. Haynes, W. M. *CRC Handbook of Chemistry and Physics*, 91st ed.; CRC Press: Boulder, CO, 2010–2011.
27. Shaya, O.; Shaked, M.; Doron, A.; Cohen, A.; Levy, I.; Rosenwaks, Y. Distinguishing between Dipoles and Field Effects in Molecular Gated Transistors. *Appl. Phys. Lett.* **2008**, *93*, 043509–3.
28. Ahn, J.-H.; Choi, S.-J.; Han, J.-W.; Park, T. J.; Lee, S. Y.; Choi, Y.-K. Double-Gate Nanowire Field Effect Transistor for a Biosensor. *Nano Lett.* **2010**, *10*, 2934–2938.
29. Choi, L.; Hong, B. H.; Jung, Y. C.; Cho, K. H.; Yeo, K. H.; Kim, D.-W.; Jin, G. Y.; Oh, K. S.; Lee, W.-S.; Song, S.-H.; Rieh, J. S.; Whang, D. M.; Hwang, S. W. Extracting Mobility Degradation and Total Series Resistance of Cylindrical Gate-All-Around Silicon Nanowire Field-Effect Transistors. *IEEE Electron Device Lett.* **2009**, *30*, 665–667.
30. Clement, N.; Nishiguchi, K.; Fujiwara, A.; Vuillaume, D. Evaluation of a Gate Capacitance in the Sub-aF Range for a Chemical Field-Effect Transistor with a Silicon Nanowire Channel. *IEEE Trans. Nanotechnol.* **2011**, *10*, 1172–1179.
31. Terada, K.; Nishiyama, K.; Hatanaka, K.-I. Comparison of MOSFET-Threshold-Voltage Extraction Methods. *Solid-State Electron.* **2001**, *45*, 35–40.
32. Yu, Y. S.; Lee, S. H.; Oh, J. H.; Kim, H. J.; Hwang, S. W.; Ahn, D. A Compact Analytical Current Conduction Model for a Depletion-Mode n-Type Nanowire Field-Effect Transistor with a Bottom-Gate Structure. *Semicond. Sci. Technol.* **2008**, *23*, 035025/1–035025/6.
33. A bare QCM resonator (without HTS-Si NWs on the surface) showed negligible response to decane exposure (*i.e.*, 0 ± 1 Hz). Therefore, it is likely that the signal obtained from the QCM measurement results from the HTS-Si NWs and to a lesser extent from the NW-free areas.
34. The Si NWs were deposited on the QCM resonators under ambient conditions containing 50–60% RH, whereas the reference air used during the QCM exposures contained 15% RH.
35. SE measurements on nanostructures are in principle possible. However, such measurements would involve elaborate modeling of the dielectric properties of the nanostructures and would require exact knowledge of the nanostructures' size and positional distribution over a macroscopic surface area, because the SE equipment used in this study probes a surface area of about 1.5 mm^2. Also, the sample surface must be free of electrodes for SE analysis.
36. Koo, S.-M.; Edelstein, M. D.; Li, Q.; ARichter, C.; Vogel, E. M. Silicon Nanowires as Enhancement-Mode Schottky Barrier Field-Effect Transistors. *Nanotechnology* **2005**, *16*, 1482–1485.
37. Sze, S. M. *Semiconductor Devices: Physics and Technology*, 2nd ed.; John Wiley & Sons, Inc.: Chichester, UK, 2001; p 568.
38. Wunnicke, O. Gate Capacitance of Back-Gated Nanowire Field-Effect Transistors. *Appl. Phys. Lett.* **2006**, *89*, 083102.
39. Fallahazad, B.; Kim, S.; Colombo, L.; Tutuc, E. Dielectric Thickness Dependence of Carrier Mobility in Graphene with HfO_2 Top Dielectric. *Appl. Phys. Lett.* **2010**, *97*, 123105/1–123105/3.
40. Jang, H.-J.; Cho, W.-J. High Performance Silicon-on-Insulator Based Ion-Sensitive Field-Effect Transistor using High-k Stacked Oxide Sensing Membrane. *Appl. Phys. Lett.* **2011**, *99*, 043703.
41. Bertiea, J. E.; Lan, Z. The Refractive Index of Colorless Liquids in the Visible and Infrared: Contributions from the Absorption of Infrared and Ultraviolet Radiation and the Electronic Molar Polarizability Below 20 500 cm^{-1}. *J. Chem. Phys.* **1995**, *103*, 10152–10161.
42. Typically, eq 9 is used to calculate the mobility from the saturation of I_{ds} *vs* V_{ds}. In this case, the obtained μ_h value depends on the $V_{th}-V_{bgs}$. To eliminate this effect, one has to calculate the mobility from the transconduction region under the same range of $V_{th} - V_{bgs}$.
43. Du, J.; Liang, D.; Tang, H.; Gao, X. P. A InAs Nanowire Transistors as Gas Sensor and the Response Mechanism. *Nano Lett.* **2009**, *9*, 4348–4351.
44. Schmidt, V.; Wittemann, J. V.; Senz, S.; Goesele, U. Silicon Nanowires. A Review on Aspects of Their Growth and Their Electrical Properties. *Adv. Mater.* **2009**, *21*, 2681–2702.
45. Mirror image charge is defined as the sum of ΔQ_s, ΔQ_D, and ΔQ_{it} of both the Si NW and substrate that cancel out ΔQ_{css} to the first-order.
46. Schmidt, V.; Senz, S.; Goesele, U. Influence of the Si/SiO_2 Interface on the Charge Carrier Density of Si Nanowires. *Appl. Phys. A: Mater. Sci. Process.* **2007**, *86*, 187–191.
47. Stelzner, T.; Andra, G.; Wendler, E.; Wesch, W.; Scholz, R.; Goesele, U.; Christiansen, S. Growth of Silicon Nanowires by Chemical Vapor Deposition on Gold Implanted Silicon Substrates. *Nanotechnology* **2006**, *17*, 2895–2898.
48. Paska, Y.; Haick, H. Controlling Surface Energetics of Silicon by Intermolecular Interactions between Parallel Self-Assembled Molecular Dipoles. *J. Phys. Chem. C* **2009**, *113*, 1993–1997.
49. Paska, Y.; Haick, H. Systematic Cross-Linking Changes within a Self-Assembled Monolayer in a Nanogap Junction: A Tool for Investigating the Intermolecular Electronic Coupling. *J. Am. Chem. Soc.* **2010**, *132*, 1774–1775.
50. Aspnes, D. E.; Theeten, J. B. Spectroscopic Analysis of the Interface Between Si and Its Thermally Grown Oxide. *J. Electrochem. Soc.* **1980**, *127*), 1359–1365.
51. Philipp, H. R. *Handbook of Optical Constants of Solids*; Academic Press, Inc.: Orlando, FL, 1985.